



Short-term clustering modeling of seismicity in Eastern Aegean Sea (Greece): a retrospective forecast test of the 2017 $M_w = 6.4$ Lesvos, 2017 $M_w = 6.6$ Kos and 2020 $M_w = 7.0$ Samos earthquake sequences

Christos Kourouklas¹ · Ourania Mangira¹ · Rodolfo Console^{2,3} · Eleftheria Papadimitriou¹ · Vassilios Karakostas¹ · Maura Murru³

Received: 8 January 2021 / Accepted: 1 April 2021 / Published online: 26 April 2021
© Institute of Geophysics, Polish Academy of Sciences & Polish Academy of Sciences 2021

Abstract

Short-term earthquake clustering properties in the Eastern Aegean Sea (Greece) area investigated through the application of an epidemic type stochastic model (Epidemic Type Earthquake Sequence; ETES). The computations are performed in an earthquake catalog covering the period 2008 to 2020 and including 2332 events with a completeness threshold of $M_c = 3.1$ and separated into two subcatalogs. The first subcatalog is employed for the learning period, which is between 2008/01/01 and 2016/12/31 ($N = 1197$ earthquakes), and used for the model's parameters estimation. The second subcatalog from 2017/01/01 to 2020/11/10 (1135 earthquakes), in which the sequences of 2017 $M_w = 6.4$ Lesvos, 2017 $M_w = 6.6$ Kos and 2020 $M_w = 7.0$ Samos main shocks are included, and used for a retrospective forecast testing based on the constructed model. The estimated model parameters imply a swarm like behavior, indicating the ability of earthquakes of small to moderate magnitude above M_c to produce their own offsprings, along with the stronger earthquakes. The retrospective evaluation of the model is examined in the three aftershock sequences, where lack of foreshocks resulted in low predictability of the mainshocks, with estimated daily probabilities around 10^{-5} . Immediately after the mainshocks occurrence the model adjusts with notable resemblance between the expected and observed aftershock rates, particularly for earthquakes with $M \geq 3.5$.

Keywords Earthquake clustering · ETES model · Aftershock sequences · Short-term earthquake occurrence probabilities · Eastern Aegean Sea

Introduction

The study of short-term spatiotemporal seismicity clustering properties constitutes a powerful tool for earthquake forecasting. These properties are being investigated via the

development of statistical models, combining well known laws of seismology, such as the Omori (1894) and Gutenberg and Richter (1949) laws. The Epidemic Type Aftershock Sequence (ETAS) is the clustering model applied to large extent for describing short-term seismicity. Introduced by Ogata (1988), this model considers the temporal seismicity properties only, and later it was also extended in their spatial clustering features (Ogata 1998). Although ETAS is the

Communicated by the Guest Editors: Ramon Zuñiga, Eleftheria Papadimitriou, Vassilios Karakostas and Onur Tan.

✉ Christos Kourouklas
ckouroukl@geo.auth.gr

Ourania Mangira
omangira@geo.auth.gr

Rodolfo Console
rodolfo.console@ingv.it

Eleftheria Papadimitriou
ritsa@geo.auth.gr

Vassilios Karakostas
vkarak@geo.auth.gr

Maura Murru
maura.murru@ingv.it

¹ Geophysics Department, School of Geology, Aristotle University of Thessaloniki, 54124 Thessaloniki, Greece

² Center of Integrated Geomorphology for the Mediterranean Area (CGIAM), Potenza, Italy

³ Istituto Nazionale Di Geofisica E Vulcanologia (INGV), Rome, Italy

most frequently used clustering model, alternative formulations also exist that describe and study the spatiotemporal clustering seismicity properties (e.g., Console and Murru 2001; Rhoades and Evison 2004; Marzocchi and Lombardi 2008).

The basic assumption upon which these models are formulated is that each earthquake, even if it is considered as foreshock, mainshock or aftershock, is capable to produce its own offspring events, depending on the previous earthquake into a time and space window, according to certain scaling relations (e.g., the aftershock productivity law). This capability has led to a large number of practical applications focusing on the characteristics of the short-term seismicity clustering properties worldwide, such as in Japan (Ogata 2011), California (Helmstetter et al. 2006; Field et al. 2017), Taiwan (Zhuang et al. 2005) and Italy (Lombardi et al. 2010; Zhuang et al. 2018).

Over the years a large number of studies were also focused on the retrospective and/or the prospective forecast of both the aftershock evolution soon after the occurrence of large main shocks and the large earthquake occurrence using small to moderate past earthquakes (Zhuang et al. 2008; Console et al. 2007; Marzocchi and Lombardi 2009; Murru et al. 2009, 2014; Ogata et al. 2013; Savran et al. 2020). The wide applicability of the candidate short-term clustering models has allowed the objective testing of their performance by the international infrastructure of Collaboratory for the Study of Earthquake Predictability (CSEP; Jordan 2006). CSEP is using reproducible prospective testing experiments to assess the performance of the candidate forecast models, in terms of the expected number of earthquakes above a specific magnitude threshold in a certain spatiotemporal window, among other metrics (e.g., Zechar et al. 2010; Rhoades et al. 2011; Schorlemmer et al. 2018).

The present study aims at the examination of the short-term seismicity clustering pattern in the Eastern Aegean Sea area via the application of the spatiotemporal model proposed by Console and Murru (2001), namely the Epidemic Type Earthquake Sequence (ETES) model, in an earthquake catalog covering the period (2008–2016; learning period) and the consistent checking of the final estimated model by the accomplishment of retrospective forecast tests in the last period since 2017 (testing period), in which the sequences of 2017 $M_w = 6.4$ Lesvos, 2017 $M_w = 6.6$ Kos and 2020 $M_w = 7.0$ Samos earthquakes are included. The verification process is performed by comparing the occurring earthquakes above certain magnitude thresholds and those that are expected according to the model.

The study area constitutes part of the back arc Aegean area (Fig. 1), exhibiting high seismic moment rates (Papazachos et al. 1997a), and frequent occurrence of large earthquakes. These characteristics offer the opportunity for thorough studies concerning the short-term clustering features

of seismicity. Console et al. (2006) applied a retrospective performance test using a spatiotemporal clustering models (both short and long term) using an earthquake catalog for the period 1981–2002 and showed that both models were performing substantially better than time-independent forecast models. Gospodinov et al. (2015) and Mangira et al. (2020) applied the temporal ETAS model and a spatiotemporal clustering model, respectively, in the central Ionian Islands area, to fit and later on to test the performance of their respective models in a retrospective way. Additional recent studies were focusing either only on temporal properties of specific seismic excitations (e.g., Mesimeri et al. 2018) or both the time and space clustering features of the Greek seismicity (Kourouklas et al. 2020).

Study area and data

The subduction of the oceanic lithosphere of Eastern Mediterranean under the continental Aegean microplate is the leading mechanism of the active deformation of the Aegean region (Papazachos and Comninakis 1971). This latter process forms the Hellenic Arc, along with the extensional back arc region of the Aegean Sea due to the roll back of the subducted plate (LePichon and Angelier 1979). The North Aegean Trough (NAT) is at the northern boundary of the Aegean microplate, representing the continuation of the westward prolongation of North Anatolian Fault (NAF) into the Aegean Sea (Fig. 1). The study area (marked by the red box in Fig. 1) constitutes the easternmost part of the Aegean Sea. The active deformation is mainly expressed by complex normal fault populations with a total extensional rate equal to 6 mm/yr (McClusky et al. 2000).

The earthquake catalog used in the current study is taken from the regional catalog of Geophysics Department of the Aristotle University of Thessaloniki (Aristotle University of Thessaloniki 1981; <http://geophysics.geo.auth.gr/ss>), by considering the recordings of the Hellenic Unified Seismological Network (HUSN) and includes crustal ($h \leq 40$ km) earthquakes with $M_w \geq 2.5$ that occurred from 1 January 2008 to 10 November 2020. The magnitudes of the catalog are expressed in moment magnitude scale (M_w) or equivalent M_w based on scaling relations proposed by Papazachos et al. (1997b). The area covered by the catalog is slightly larger than the study area (at least 0.2° at all dimensions), for avoiding any possible boundary effect in the application of the clustering model.

The completeness magnitude is investigated with the Goodness-of-Fit method (GFT; Wiemer and Wyss 2000), considering the 95% confidence level of residuals (Fig. 2a). Even though the first magnitude bin with less than 5% of residuals was found equal to $M = 2.9$ (residuals = 4.54%), the completeness magnitude, M_c , was considered equal to

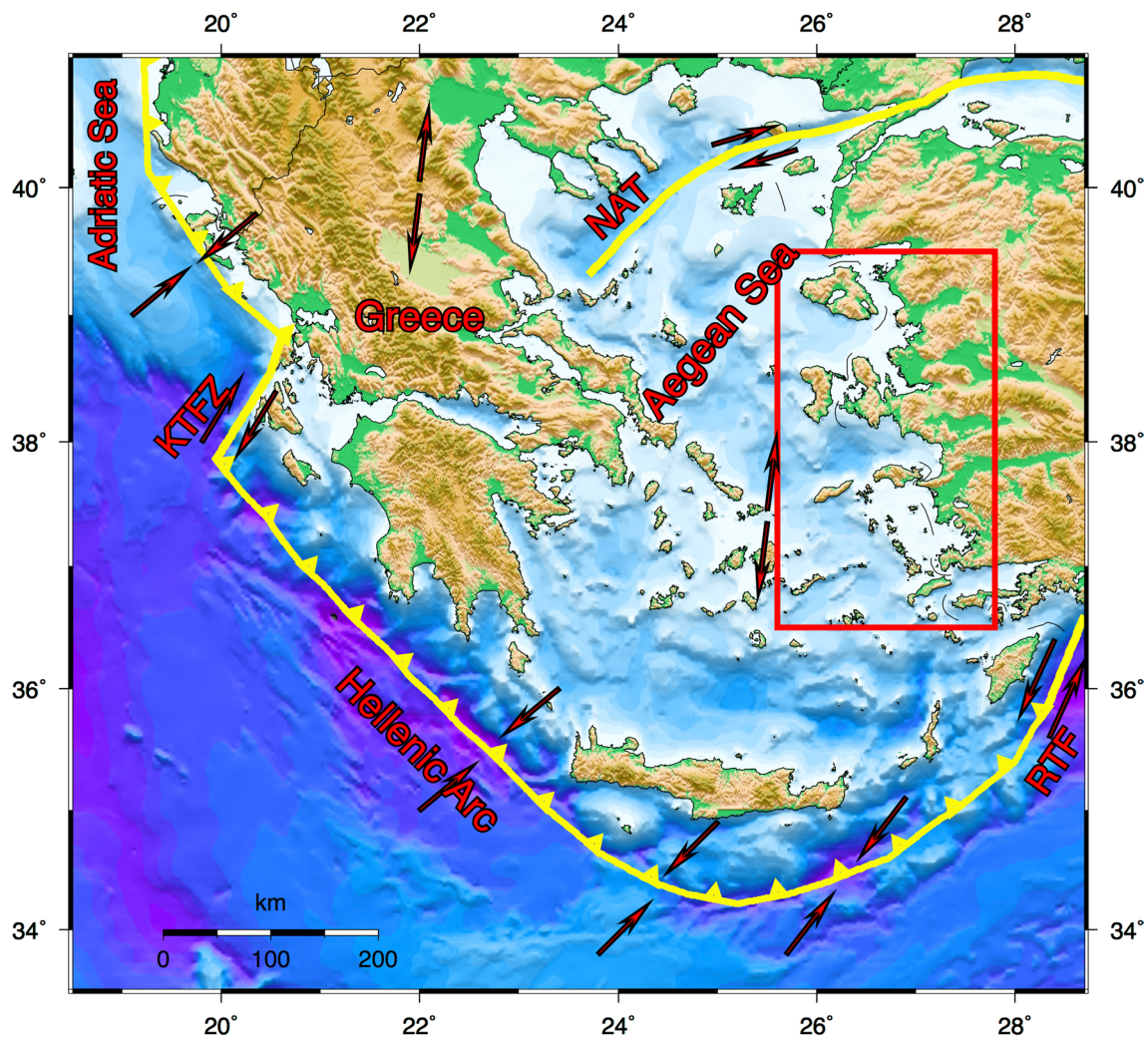


Fig. 1 The active boundaries (solid yellow lines) and their relative motions (red arrows) in the broader Aegean Sea area. The study area is denoted with the red rectangle. The epicenters of the 12 June 2017 $M_w=6.4$ (Event 1) and the 20 July 2017 $M_w=6.6$ (Event 2) earth-

quakes occurred in Lesvos and Kos islands are depicted by yellow stars, while the one of the $M_w=7.0$ 30 October 2020 Samos earthquake by a red star (Event 3)

3.1 ($M_c=3.1$), with the minimum value of residuals equal to 2.75%, resulting to a data set with 2332 earthquakes of $M \geq 3.1$. The selection of the magnitude bin of 3.1, which performs the least residual percentage according to the GFT method, is made to ensure the most reliable and secure data sample for the model application. This is clearer from Fig. 2b, focusing on to the incremental number of earthquakes (orange circles), where between the magnitude bins of $M=2.9$ and $M=3.1$ the earthquake frequency is not increasing steadily. From the $M_c=3.1$ and beyond the magnitude distribution appears consistent.

The b -value is estimated via the maximum likelihood method (Aki 1965) and takes a value of $b=1.10 \pm 0.005$, and the total seismicity rate above M_c , a , is found equal to 6.77 ($a=6.77$) after applying the Gutenberg–Richter law to the data above M_c . The b -value standard error was computed

with the method proposed by Shi and Bolt (1982). The fit of the Gutenberg–Richter law using the estimated seismic parameters b and a to the final dataset (Fig. 2b) reveals a deficit of moderate to large earthquakes, namely in the magnitude range $5.5 \leq M_w < 6.4$, during the period 2008–2020.

The study area is characterized by moderate seismicity rates with small to moderate magnitudes during the period since 2008 until the May of 2017 (Figs. 3 and 4), with only some swarm excitations like the one occurred southeastern of the Samos Island during 2009 with largest earthquake magnitude equal to $M_w=5.1$ (Tan et al. 2014). During June and July of 2017, two large ($M_w \geq 6.0$) earthquakes occurred in the northern and southern borders of the study area, respectively. Specifically, on the 12th of June 2017 a large ($M_w=6.4$) main shock (Event 1 in Fig. 1 and Table 1) occurred offshore the south-east coast of Lesvos Island. The

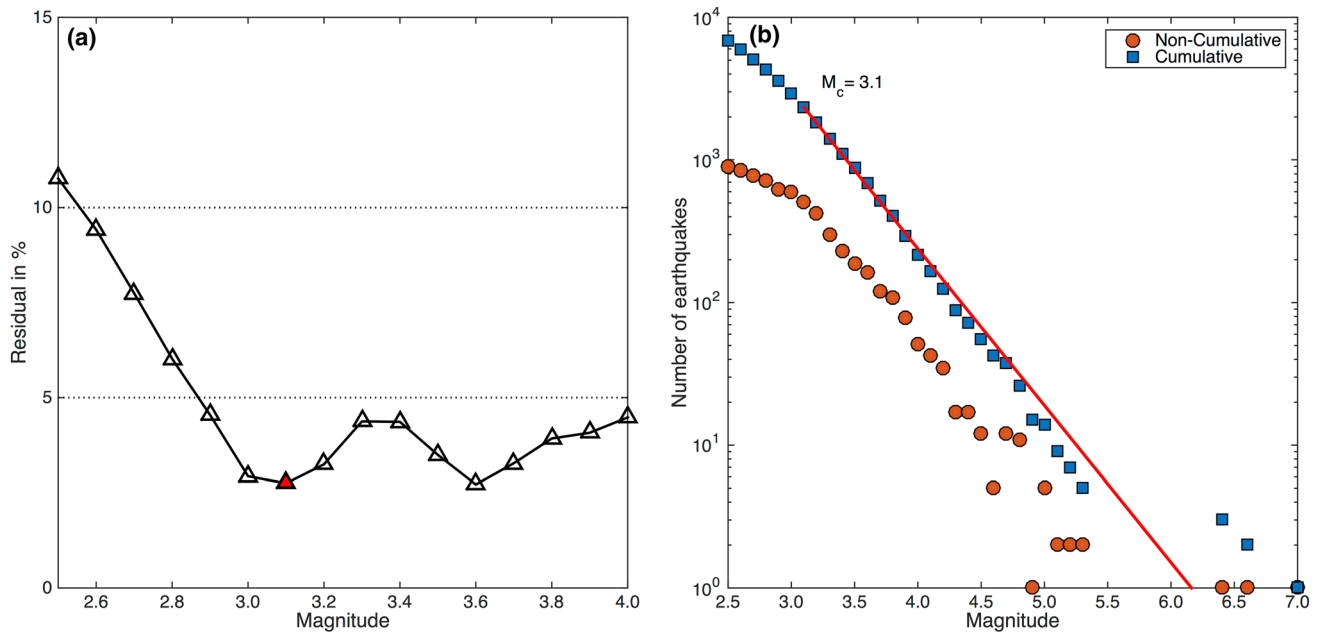


Fig. 2 Magnitude of completeness, M_c , calculation via the Goodness-of-Fit (GFT) method for the period 1 January 2008 to 10 November 2020. **a** The percentage of residuals (100-R) between the observed frequency-magnitude distributions and the ideal synthetic power law as a function of the minimum magnitude cut-off of the catalog. The

red triangle indicates the magnitude bin with the least residual value (2.75%). **b** The Magnitude-Frequency Distribution (MFD) of the incremental and the cumulative number of events (orange circles and blue squares, respectively). The red straight line represents the MFD part above the magnitude of completeness

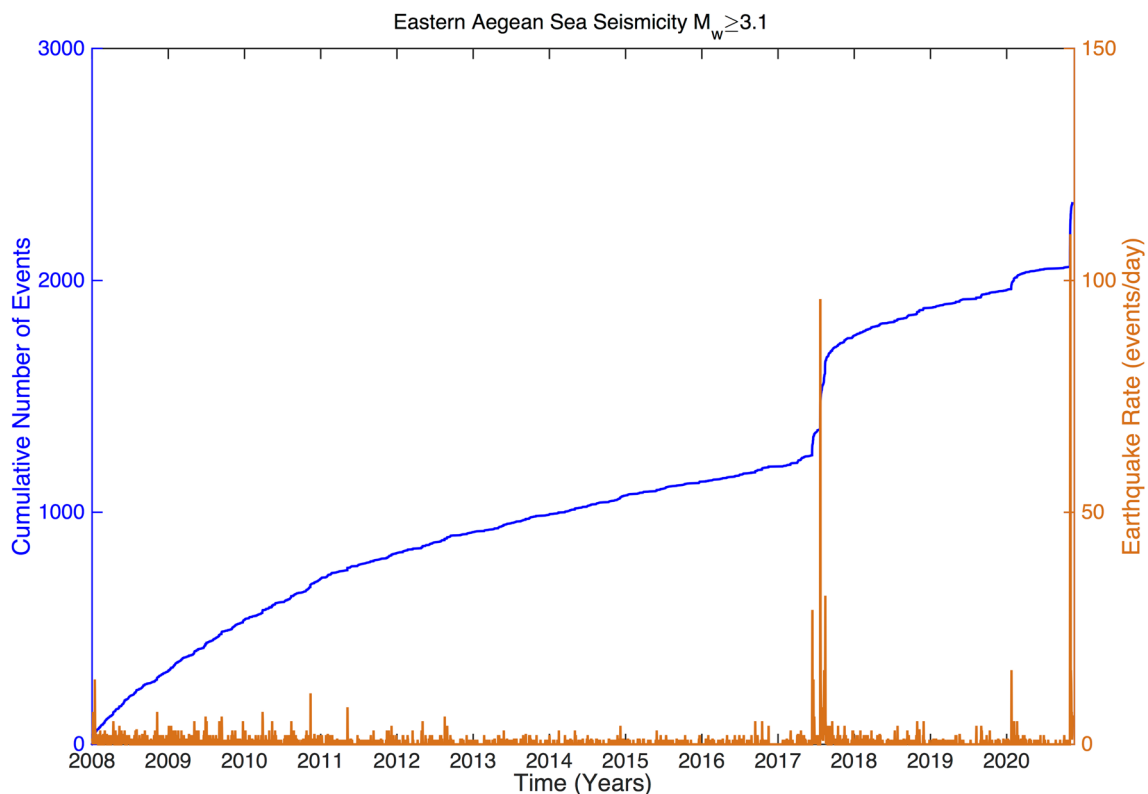


Fig. 3 Cumulative number of earthquakes (left y axis; blue line) and daily earthquake rate (right y axis; orange line) with magnitudes above M_c ($M_c = 3.1$) during the period 1 January 2008 to 10 November 2020 versus time

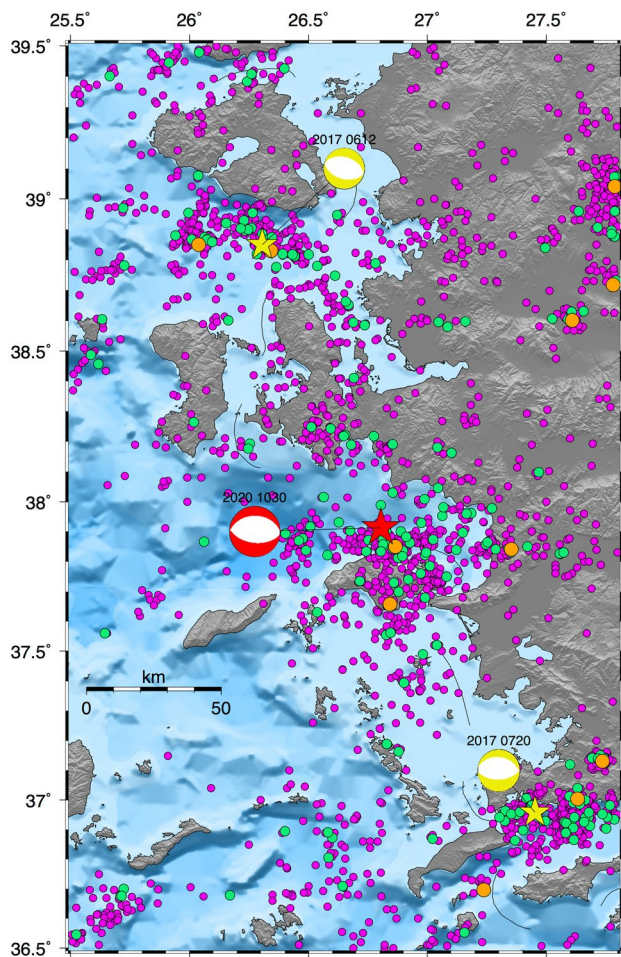


Fig. 4 Epicentral distribution of the crustal ($0 \text{ km} \leq h \leq 40 \text{ km}$) earthquakes occurred in the study area with magnitudes above M_c ($M_c = 3.1$) during the period 1 January 2008 to 10 November 2020. Small magenta, moderate green and large orange circles represent the $3.1 \leq M_w < 4.0$, $4.0 \leq M_w < 5.0$ and $5.0 \leq M_w < 6.0$ earthquakes. Yellow stars are depicting the $M_w \geq 6.0$ earthquakes, whereas the red star the $M_w = 7.0$ earthquake

mainshock was followed by many aftershocks (about 900 events, with M ranging from 1.2 to 5.2), with the largest of them being equal to $M_w = 5.2$ (Papadimitriou et al. 2018). Aftershocks concentrated in an area striking NW–SE and extending about 40 km, parallel to the south-east coasts of Lesbos Island. A second large main shock with $M_w = 6.6$ occurred on the 20th of July 2017 (Event 2 in Fig. 1 and Table 1) offshore, north of the Kos Island, strongly felt and damaged cities on the Island and the town of Bodrum in the

Table 1 Strong ($M_w \geq 6.0$) earthquakes focal parameters occurred in the Eastern Aegean Sea since 2017

Event Number	Date (yyyy-mm-dd)	Origin Time	Lat. (°E)	Lon. (°N)	Depth (km)	M_w	Region
01	2017-06-12	12:28:38.70	38.849	26.305	08.50	6.4	Lesvos Isl
02	2017-07-20	22:31:10.80	36.959	27.453	12.00	6.6	Kos Isl
03	2020-10-30	11:51:25.48	37.913	26.803	12.93	7.0	Samos Isl

western Turkey coastline. The aftershock activity extended on both sides of the mainshock epicenter with many aftershocks within two weeks after its occurrence (Ganas et al. 2019).

Earthquake rates decreased within the study area soon after the extinction of the second 2017 strong earthquake sequence to values like the pre 2017 excitations level during the years 2018–2020, until the occurrence of the 2020 Samos ($M_w = 7.0$) main shock (Fig. 3), which occurred offshore the northern coasts of Samos island (Event 3 in Fig. 1 and Table 1). The daily earthquake rates were significantly increased (Karakostas et al. 2020), exhibiting the largest values observed during the whole study period. A large number of aftershocks occurred immediately after the main shock, with 6 of them having magnitudes $4.0 \leq M_w < 5.0$ within only 15 min. Aftershocks activity occupied an area extending more than 50 km in an E–W direction offshore the northern coasts of Samos island (Fig. 4).

In summary, Eastern Aegean seismicity could be divided into two distinctive periods of activity, one with moderate occurrence rates until the first half of 2017 and a second one dominated by the occurrence of the seismic sequences in 2017 and 2020. These two periods constitute the duration of the two subcatalogs of our investigation. The first subcatalog comprises earthquakes that occurred from 2008/01/01 to 2016/12/31, accounting for the learning period ($N = 1197$ earthquakes), and will be used for the parameters estimation of the clustering model. The seismic sequences are included into the second subcatalog (testing period catalog), lasting from 2017/01/01 to 2020/11/10 and including 1135 earthquakes, which will be later used for the retrospective forecasting tests using the estimated model parameters of the learning period.

ETES model formulation

The short-term clustering features of seismicity are investigated with the application of the Epidemic Type Earthquake Sequence (ETES) stochastic model. The ETES model had been formulated by Console and Murru (2001) and further improved and discussed by Console et al. (2003). In this section, a brief outline including its main principles is presented.

Seismicity on short-scale is considered clustered in time and space. On short scale oftentimes the terms foreshock,

main shock and aftershock are arbitrarily used, and their distinction is difficult, therefore, the adoption of an appropriate model where events are not labeled is necessary. Earthquakes are considered as elements in a self-exciting point process called Hawkes' process. Each one of them corresponds to a point with coordinates (x, y, t, m) corresponding to the event's location, time, and magnitude, respectively. Depth is ignored not only for simplicity but also due to the uncertainties associated with its computations.

The fundamental idea of the model is the potential triggering of every event by the previous ones and its capability to trigger subsequent events in line with their relative time and space distance. Seismicity is the summation of background spontaneous and offspring events as it is depicted in the form of the expected rate density, λ ,

$$\lambda(x, y, t, m) = f_r \lambda_0(x, y, m) + \sum_{i=1}^N H(t - t_i) \lambda_i(x, y, t, m)$$

$$\text{with } H(t) = \begin{cases} 0, & \text{if } t \leq 0 \\ 1, & \text{if } t > 0 \end{cases} \quad (1)$$

where f_r is the ratio of the earthquakes that are considered independent, defined as the "failure rate", $\lambda_0(x, y, m)$ is the background seismicity, t_i is the occurrence time of i th event and N is the total number of earthquakes and $\lambda_i(x, y, t, m)$ is the function expressing the contribution of the previous events according to the magnitude, distance and time of the triggering earthquake (Console and Murru 2001; Console et al. 2003).

The first term of the summation refers to the time-independent seismicity and the second term to the time-dependent "induced" seismic activity. This relation reveals the concept of the ETES model, i.e., the assumption that no earthquake should be considered absolutely independent or dependent on a particular previous event. On the contrary, every earthquake is connected based on different weights to all previous ones as well as to the background seismicity.

The long-term background seismicity, $\lambda_0(x, y, m)$ is computed when ignoring the interactions between earthquakes under the assumption that the Gutenberg–Richter law holds. It takes the form

$$\lambda_0(x, y, m) = \mu_0(x, y) \beta e^{-\beta(m-m_0)}, \quad (2)$$

where $\mu_0(x, y)$ is the background seismicity spatial kernel density of events with magnitude $m \geq m_0$ and $\beta = b \ln(10)$. The background spatial density $\mu_0(x, y)$ is computed with the method of Frankel (1995) by means of a smoothing algorithm developed by Console et al. (2010). According to this algorithm, earthquakes are weighted by the probability of being independent, as it is also suggested by Zhuang et al. (2002). Then, the weights are adapted through an iterative process.

Regarding the single contribution of the previous events, the term $\lambda_i(x, y, t, m)$ comprises the time, magnitude and space distribution, as follows

$$\lambda_i(x, y, t, m) = Kh(t - t_i) \beta e^{-\beta(m-m_i)} f(x - x_i, y - y_i), \quad (3)$$

where K is a constant parameter, namely the productivity coefficient, $h(t)$ and $f(x, y)$ are the temporal and spatial functions. The modified Omori law (Ogata 1983) describes the time dependence

$$h(t) = (p - 1)c^{p-1}(t - c)^{-p}, \quad p > 1, \quad (4)$$

where c and p are the parameters of the point process. For the spatial component of the triggered earthquakes several forms have been proposed (Zhuang et al. 2002, 2004, 2005; Ogata & Zhuang 2006; Console et al. 2006).

A function $f(x - x_i, y - y_i)$ with circular symmetry around the point (x_i, y_i) is adopted in this study following Console et al. (2003). It can be written in polar coordinates (r, θ)

$$f(r, \theta) = \frac{(q - 1)}{\pi} \frac{d'^{2(q-1)}}{(r^2 + d'^2)^q}, \quad (5)$$

where r is the distance between points (x, y) and (x_i, y_i) , q is a free parameter, $d' = d_0 e^{\alpha(m_i - m_0)}$ where d_0 is the characteristic triggering distance for an event with magnitude m_i and α is a free parameter.

The ETES model parameters (K, d_0, q, α, c and p) are estimated through the maximum-likelihood estimation method. It should be noted that the parameter f_r , i.e., the fraction of the events that are considered independent is not free. It is restricted by the fact that the two parts of Eq. (1), the observed and expected number of events are equal.

Application of ETES model for the learning period (2008/01/01 to 2016/12/31)

The initial step, which is a prerequisite for the estimation of the model's parameters, is the estimation of the correlation distance, C , of the epicentral distribution of the earthquakes in the learning period. The correlation distance could be considered as an indicator of the spatial variability of seismicity, i.e., showing the spatial interrelation of the earthquakes. The correlation distance is then used to estimate the smoothed distribution of the background seismicity. This estimation is made by the application of a smoothed seismicity algorithm proposed by Console et al. (2010) using the spatial kernel method of Frankel (1995). In this way, the learning period catalog is divided into two almost equal parts, the first part with 601 earthquakes and the second part with 596 earthquakes, and various correlation distances are tested assuming the Poisson model using the second part

over the first part and vice versa (Fig. 5). The optimal correlation distances, C_1 and C_2 , are then selected in accordance with their respective log likelihood values and found equal to $C_1 = 15$ km and $C_2 = 17$ km. The final correlation distance, C , for the entire learning period is the average value of C_1 and C_2 , namely equal to 16 km ($C = 16$ km).

The estimation of the ETES model parameters is implemented via an iterative procedure described in detail by Console et al. (2010). As a first step the maximum likelihood estimation method is applied to the initial smoothed seismicity distribution, which is obtained from the average correlation distance of 16 km (Fig. 6a). These estimates (K , d_0 , q , α , c and p , along with f_r ; Table 2) are then used for the calculation of the probability of an event to belong either to the time-independent or the triggered seismicity and a new weighted smoothed distribution is estimated based on these probabilities (Fig. 6b). A new set of parameters is estimated by means of the weighted distribution and the procedure was repeated until the optimal set is found (i.e. the set which has the maximum likelihood value over all the iterations).

In our case the optimal set of the ETES parameters is found at once, since the second iteration results in a lower likelihood value. However, a third round of the iterative procedure is made to ensure the convergence of the parameters' estimation. The optimal set of parameters is shown in Table 2. The proportion of the expected background events over the total number of events is found equal to 0.502 ($f_r = 0.502$), showing that half of the learning period earthquakes belong to the background seismicity. Productivity

coefficient K ($K = 0.105$) is found to be rather high compared with previous studies (e.g., Mangira et al. 2020), showing that small earthquakes with magnitudes above the M_c are capable to produce their own triggered events. The estimated productivity parameter α ($\alpha = 0.419$) value is about half of the typical one ($\alpha \approx 0.8$) as found for Mainshock–Aftershock sequences (de Arcangelis et al. 2016, among others) This is probably attributed to earthquakes included in the learning period, which is dominated by small to moderate magnitude earthquakes rather than by strong (e.g., $M_w \geq 6.0$) ones. This implies that the ability of the offspring events production is also controlled by moderate magnitude events and not only by the stronger ones (Fig. 7a).

The estimated temporal parameters of the modified Omori law, the c and p for the learning period ($c = 8.893e-3$ and $p = 1.012$) result in an effective time interval of about 10 days in which the aftershock occurrence rate is high. After this time, the occurrence probability of aftershocks significantly diminishes in relation to their rate being almost equal to zero (Fig. 7b). The value of the characteristic triggering distance, d_0 , ($d_0 = 2.541$ km) of an event with $M = M_c$ combined with the productivity parameter, α , which included a spatial triggering response function, scaled to an event magnitude, indicates that a $M = 5.0$ earthquake will affect a circular area with a radius of about 16 km, whereas a $M_w = 6.0$ earthquake affects an area of almost 40 km radius with direct aftershocks. The value of spatial decay of offspring events, q , is found equal to 1.932 ($q = 1.932$).

Although the estimated model parameters are based on a learning period catalog dominated by small to moderate

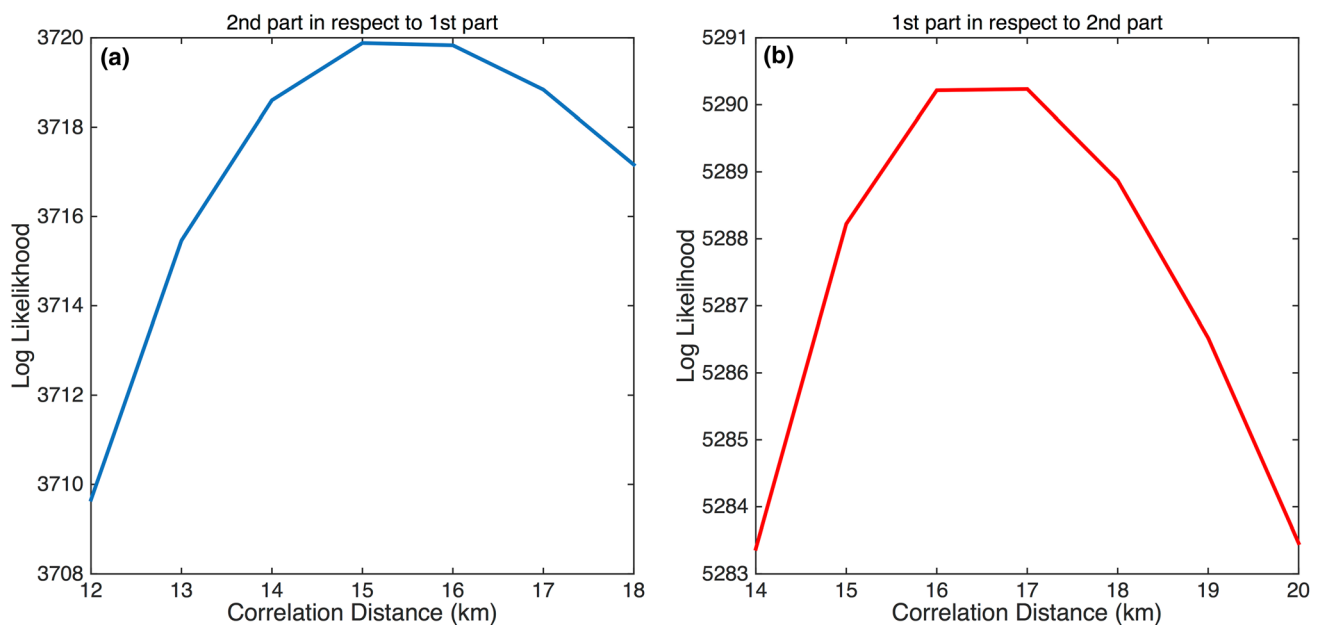


Fig. 5 **a** Likelihood of the Poisson model against the correlation distance, C , in km of the second part of the catalog of the learning period over the first part as obtained from the smoothing approach. **b** Same as (a) for the first part of the catalog of the learning period over the second part

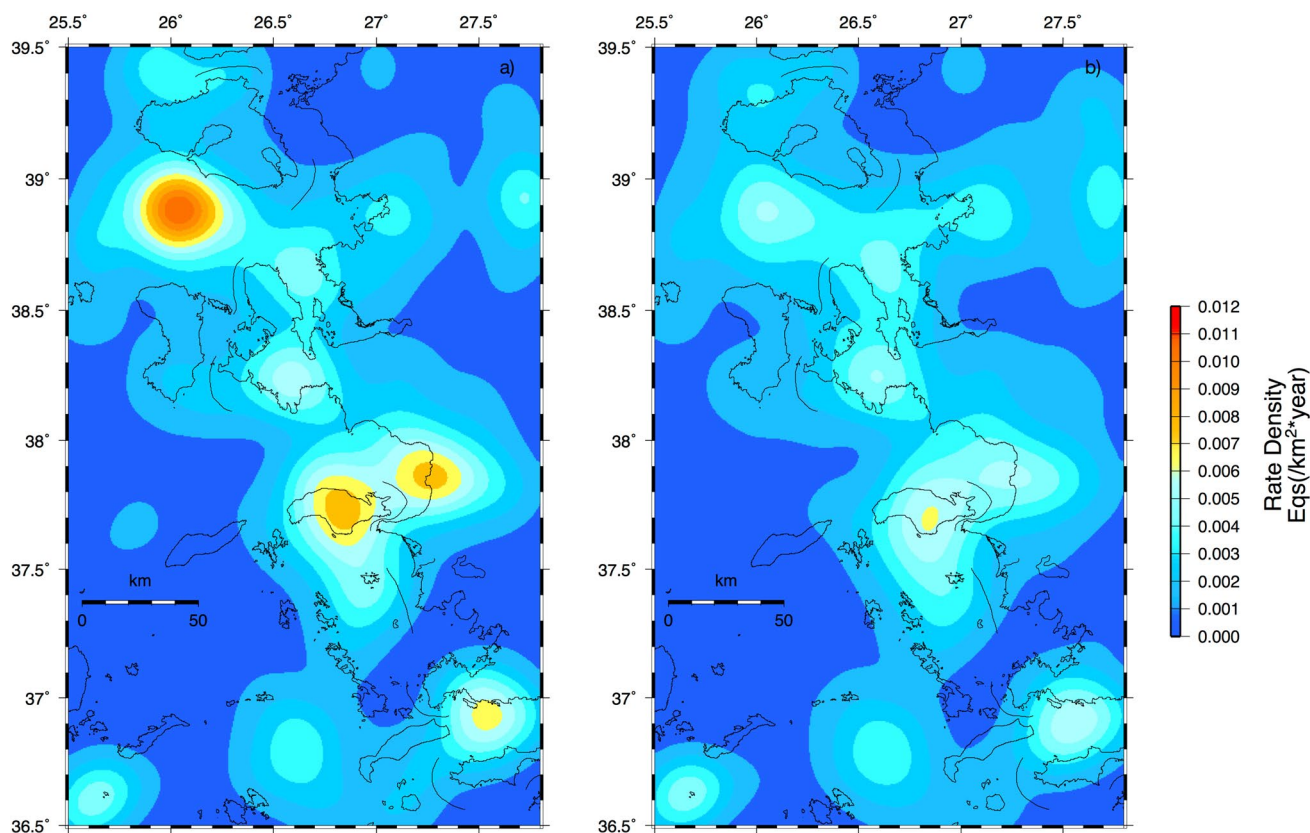


Fig. 6 Smoothed seismicity of the Eastern Aegean Sea during the learning period (1 January 2008 to 31 December 31) as obtained from the smoothing approach using the average correlation distance

($C = 16$ km) for the initial catalog (a) and the weighted one (b) after the parameters estimation of the model

Table 2 ETES parameters estimate for the Eastern Aegean Sea using the learning period (2008/01/01 to 2016/12/31) dataset

Iteration	f_r	$K (d^{p-1})$	d_0 (km)	q	c (d)	p	α	Log likelihood
1	0.502	0.105	2.541	1.932	8.893E-3	1.012	0.419	11,642.2598
2	0.474	0.106	2.596	1.943	9.817E-3	1.012	0.421	11,625.7529
3	0.474	0.108	2.596	1.942	9.817E-3	1.012	0.421	11,625.5322

events, which exhibit a more swarm like behavior rather than a Mainshock–Aftershock one, the validation of the model using the testing period data is an interesting task that will be investigated in the next section.

Retrospective testing of the model with the 2017 $M_w = 6.4$ Lesvos, 2017 $M_w = 6.6$ Kos and 2020 $M_w = 7.0$ Samos earthquake sequences

As previously mentioned, the duration of the learning period lasts from the 1st of January 2008 until the 31st of December 2016, while the testing period starts on the 1st of January 2017 and terminates on the 10th of November 2020. The testing period, includes the 2017 $M_w = 6.4$ Lesvos and

the 2017 $M_w = 6.6$ Kos aftershock sequences and terminates soon after the initiation of the 2020 $M_w = 7.0$ Samos sequence, for which a retrospective test will be performed on the model capability to forecast the daily aftershock rate. For a direct comparison of the model performance, it is necessary to use the same set of parameters.

The testing period for the 2020 Samos seismic sequence is chosen to be between the 1st of September and the 10th of November 2020. For every day of the testing period daily occurrence probabilities are calculated for aftershocks with various magnitude thresholds. The absence of foreshocks is reflected in the calculations since, before the occurrence of the mainshock, the values of the occurrence probabilities for earthquakes with $M \geq 3.5$ are almost stable and about 5×10^{-2} and for events with $M \geq 4.5$ about 3×10^{-3} . For this reason at the midnight of the last day, approximately

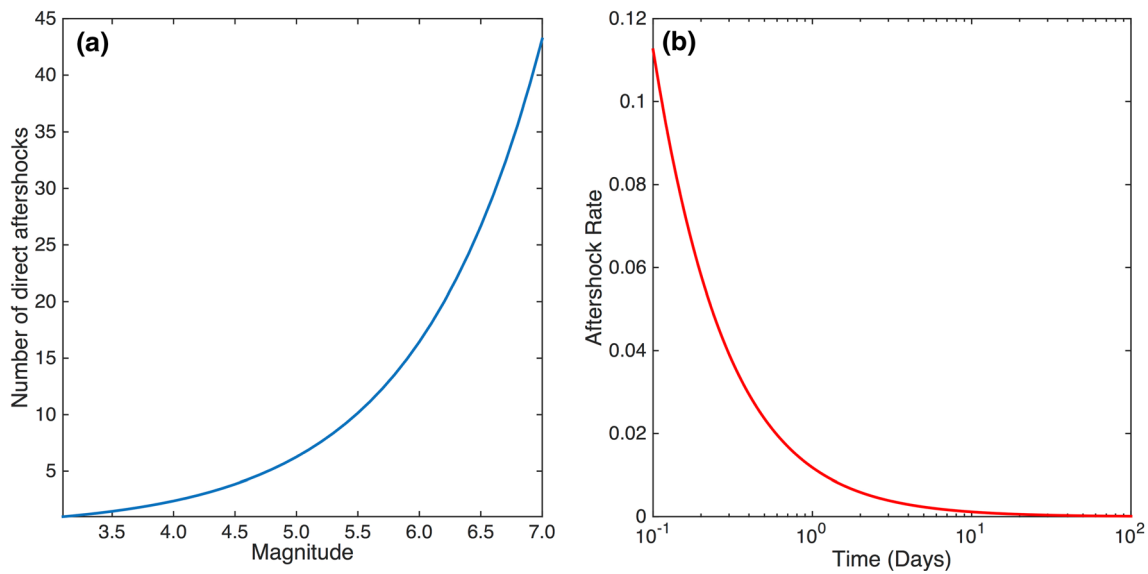


Fig. 7 Number of direct offsprings versus the corresponding triggering magnitude (a) and the temporal aftershocks decay (b) versus time, using the obtained parameters of the ETES model

12 h before the occurrence of the $M_w = 7.0$ main shock, the occurrence probability for an event with $M \geq 6.5$ in the entire study area was found equal to 1.1×10^{-5} . The daily occurrence probabilities for events with $M \geq 3.5$ and $M \geq 4.5$ for several days before and after the mainshock are presented in Fig. 8a. A large difference is observed between the calculations before and after the main shock occurrence (red dotted line). Particularly, earthquakes with $M \geq 3.5$ are expected to occur with a probability almost equal to 1 for the days after the mainshock. The daily probabilities of an event with $M > 4.5$ decrease gradually after the 31st of October since zero events in that magnitude range are observed after that date.

A large discrepancy is also observed when comparing the expected and the observed number of earthquakes that occurred on the 30th of October. The calculations are performed at the midnight of the last day before the mainshock occurrence and refer to the earthquake occurrence of the entire day. Yet, the model is quickly adjusted from the second day and the number of observed toward the expected events are well coincided for earthquakes with $M \geq 3.5$ (Fig. 9b) and those with $M \geq 4.5$ (Table 3). Particularly on the 31st of October they are remarkably similar (32.47 expected events Vs 33 observed events with $M \geq 3.5$ and 1.89 expected events Vs 1 observed events with $M \geq 4.5$).

The location of the observed earthquakes and their relationship with the expected ones is investigated through occurrence rate density time-dependent maps which illustrate the spatial pattern of the expected events. The computations are daily and are performed in cells of $0.1^\circ \times 0.1^\circ$.

Again, good agreement between the forecast and the observations is established soon after the mainshock occurrence (Fig. 10).

The evolution of the 2017 Kos seismic sequence, located at the southern border of the study area, is also tested retrospectively. The verification period covers the 31 days of July 2017, with the main shock occurred on the 21st of July. Twelve (12) events with $M \geq M_c$ occurred in the testing period before the $M_w = 6.6$ Kos main shock. For this reason, the daily occurrence probabilities of $M \geq 3.5$ events are slightly larger than in the previous case, ranging from 0.05 to 0.16. The occurrence probabilities for an event with $M \geq 4.5$ range between 0.003 and 0.01. After the 21st of July, like in the case of Samos sequence, the daily occurrence probability of an earthquake with $M \geq 3.5$ is almost equal to 1. For events with $M \geq 3.5$ the occurrence probabilities drop relatively fast and reach the value of 0.1 (Fig. 8b).

On the 20th of July, the occurrence day of the mainshock, 18 events with $M \geq 3.5$ occurred. The aftershock sequence is not as rich as in the previous examined case, but this is also happening because the mainshock occurred approximately 2 h before the beginning of the computations of the day after. In the day after the occurrence of the mainshock the difference between the observed and the expected number of events is marginal (45.28 expected toward 44 observed events) (Fig. 9b, Table 4). The spatial pattern of the expected earthquakes rates agrees well with the aftershocks locations (Fig. 11).

The 2017 $M_w = 6.4$ Lesvos sequence is located in the northern part of the study area. The testing period lasts from

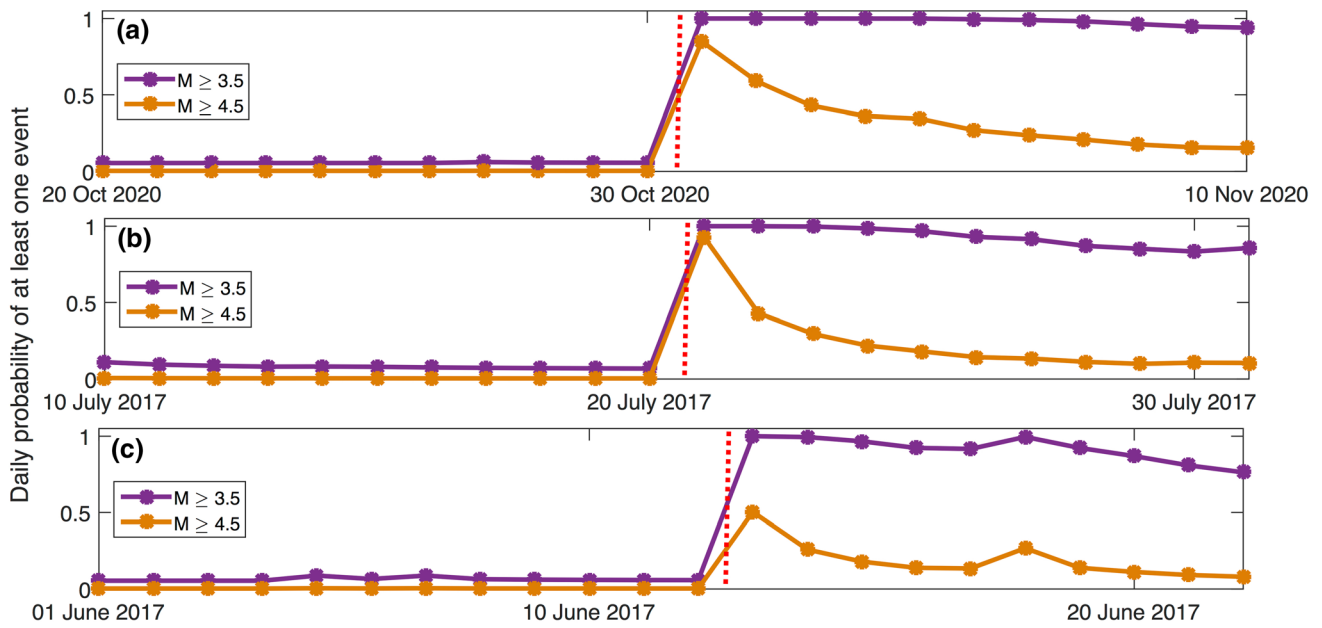


Fig. 8 Occurrence probability per day of at least one event with $M \geq 3.5$ and $M \geq 4.5$ with magenta and orange lines, respectively, for several days before and after **a** the 2020 $M_w = 7.0$ Samos earthquake, **b** the 2017 $M_w = 6.6$ Kos earthquake, **c** the 2017 $M_w = 6.4$ Lesvos earthquake. The red dotted lines coincide with the mainshocks

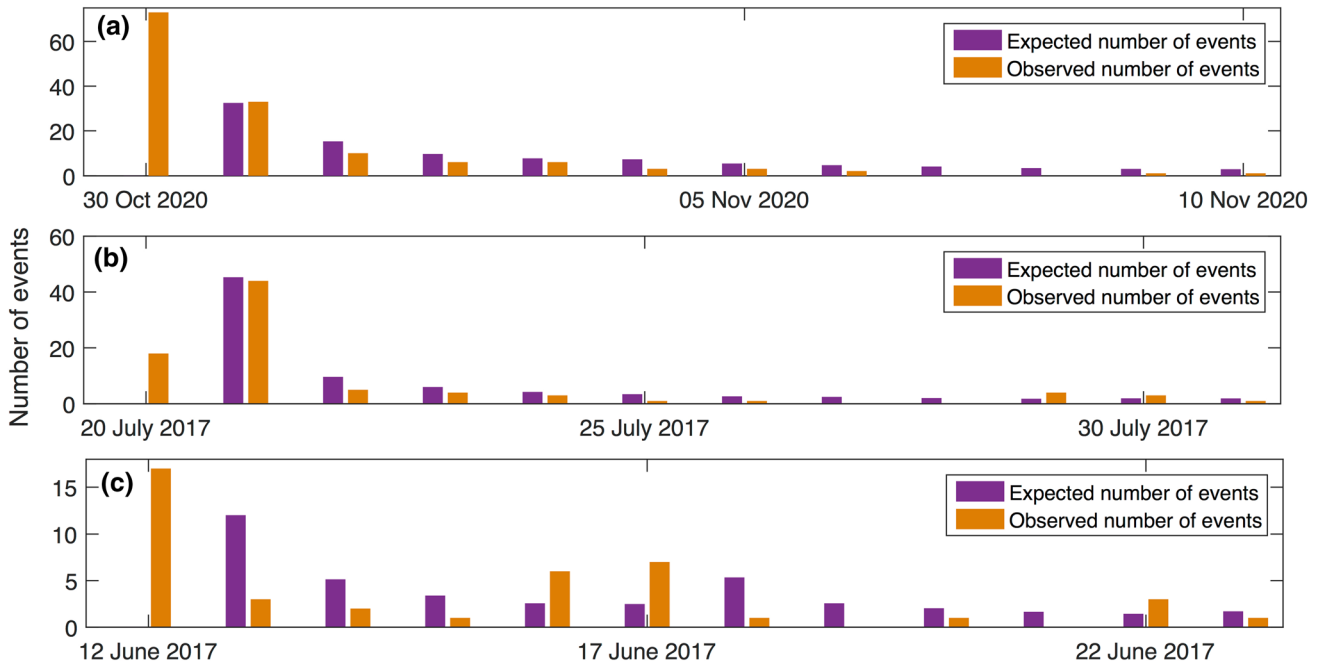


Fig. 9 Expected versus observed number of events with $M \geq 3.5$ under the clustering model for **a** the 2020 $M_w = 7.0$ Samos sequence, **b** the 2017 $M_w = 6.6$ Kos sequence, **c** the 2017 $M_w = 6.4$ Lesvos sequence

the 1st of June until the 30th of June 2017. Before the mainshock occurrence only 2 events with $M \geq M_c$ are included in the verification period. This is the reason that at midnight,

approximately 12 h prior to the $M_w = 6.4$ event the occurrence probability for an $M \geq 6.0$ earthquake is relatively low, 4.8×10^{-5} . The daily occurrence probabilities of events with

Table 3 Expected and observed number of events with $M \geq 3.5$ and $M \geq 4.5$ per day under the clustering model for Samos sequence

Date	Number of events with $M \geq 3.5$		Number of events with $M \geq 4.5$	
	Expected	Observed	Expected	Observed
30 October 2020	0.05	73	0.0036	7
31 October 2020	32.47	33	1.89	1
01 November 2020	15.28	10	0.89	0
02 November 2020	9.65	6	0.56	0
03 November 2020	7.68	6	0.44	0
04 November 2020	7.24	3	0.42	0
05 November 2020	5.37	3	0.31	0

$M \geq 3.5$ and $M \geq 4.5$, are shown in Fig. 8c with magenta and orange lines, respectively. A $M_w = 5.3$ event on the 17th of

June and its own aftershocks is responsible for the increase that is observed in the daily probability calculations on the 18th of June. This fact is also reflected when comparing the expected and observed number of events (Fig. 9c). At first, the expected number of events is larger than the observed one, but the ongoing seismic activity is responsible for the increase in the expected rates. The expected number of events per day per cell of $0.1^\circ \times 0.1^\circ$ is in good agreement with the observations (Fig. 12, Table 5).

Discussion and conclusions

The short-term clustering features of the Eastern Aegean Sea (Greece) seismicity are studied by applying an epidemic type stochastic model, namely the ETES model. The application

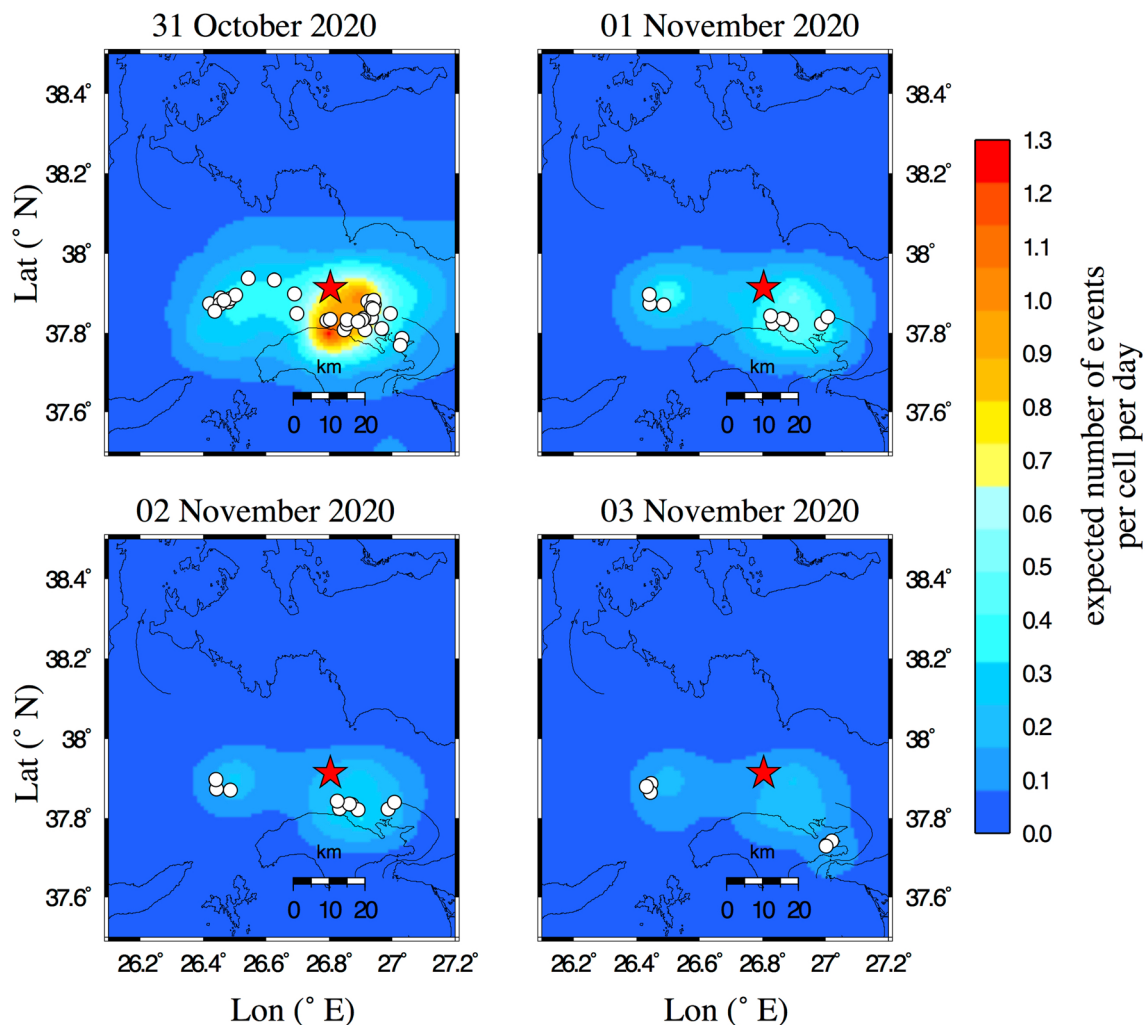


Fig. 10 Expected number of events with $M \geq 3.5$ related to the Samos sequence per day per cell of $0.1^\circ \times 0.1^\circ$ from 31 October until 03 November 2020. The starting time for the daily computations is at

midnight. The epicenters of the occurring shocks are represented with white circles. The red star represents the epicenter of the $M_w = 7.0$ Samos earthquake that occurred on 30 October 2020

Table 4 Expected and observed number of events with $M \geq 3.5$ and $M \geq 4.5$ per day under the clustering model for Kos sequence

Date	Number of events with $M \geq 3.5$		Number of events with $M \geq 4.5$	
	Expected	Observed	Expected	Observed
20 July 2017	0.07	18	0.0041	1
21 July 2017	45.28	44	2.64	3
22 July 2017	9.64	5	0.56	1
23 July 2017	5.99	4	0.35	0
24 July 2017	4.23	3	0.24	0
25 July 2017	3.42	1	0.19	0
26 July 2017	2.65	1	0.15	0

is performed using an earthquake catalog covering the period 2008–2016. The learning phase (2008–2016), is characterized by moderate seismicity rates of earthquakes with small to moderate magnitudes up to $M_w = 5.1$. The estimation of

the ETES model parameters reveals a property of moderate magnitude events to produce their own triggered events.

The retrospective testing of the ETES model performance is motivated by the recently occurred 2020 $M_w = 7.0$ Samos earthquake sequence. The remarkably close temporal proximity of two sequences in the northern and southern borders of the study area, near Lesvos and Kos islands, during 2017 has provided the opportunity to compare the fitting and investigate the adjustment of the model in the spatiotemporal behavior of the three sequences. The performed tests also focused on the reliability of the forecasts regarding the mainshocks.

For all examined cases, the absence of foreshocks has been the reason for the low predictability performance for the mainshocks occurrence, with the occurrence probabilities to be around 10^{-5} . The model though soon adjusts, from the second day of the sequences and computations, with notable resemblance between the number of observed earthquakes and those obtained from the retrospective

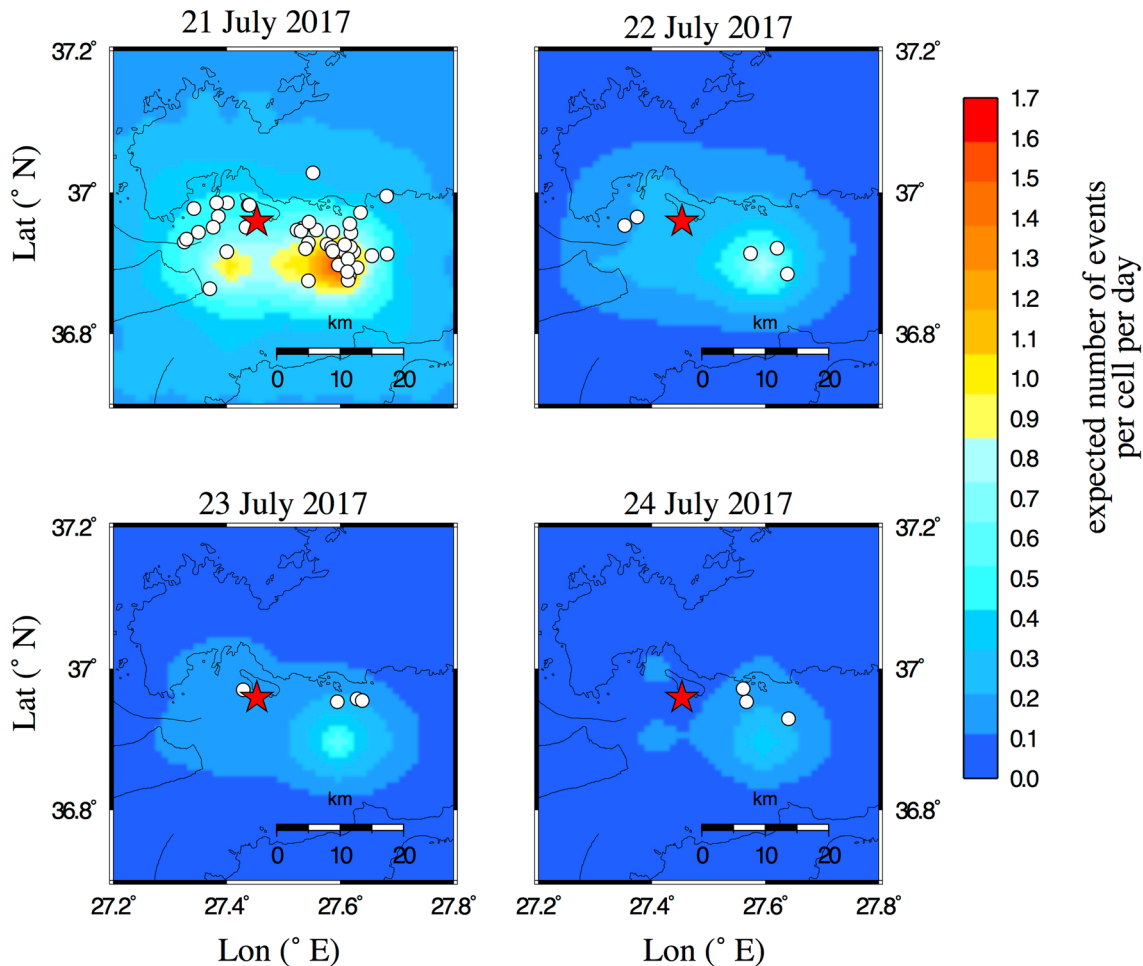


Fig. 11 Expected number of events with $M \geq 3.5$ related to the Kos sequence per day per cell of $0.1^\circ \times 0.1^\circ$ 21 July until 24 July 2017. The starting time for the daily computations is at midnight. The epi-

centers of the occurring shocks are represented with white circles. The red star represents the epicenter of the $M_w = 6.6$ Kos earthquake that occurred on 20 July 2017

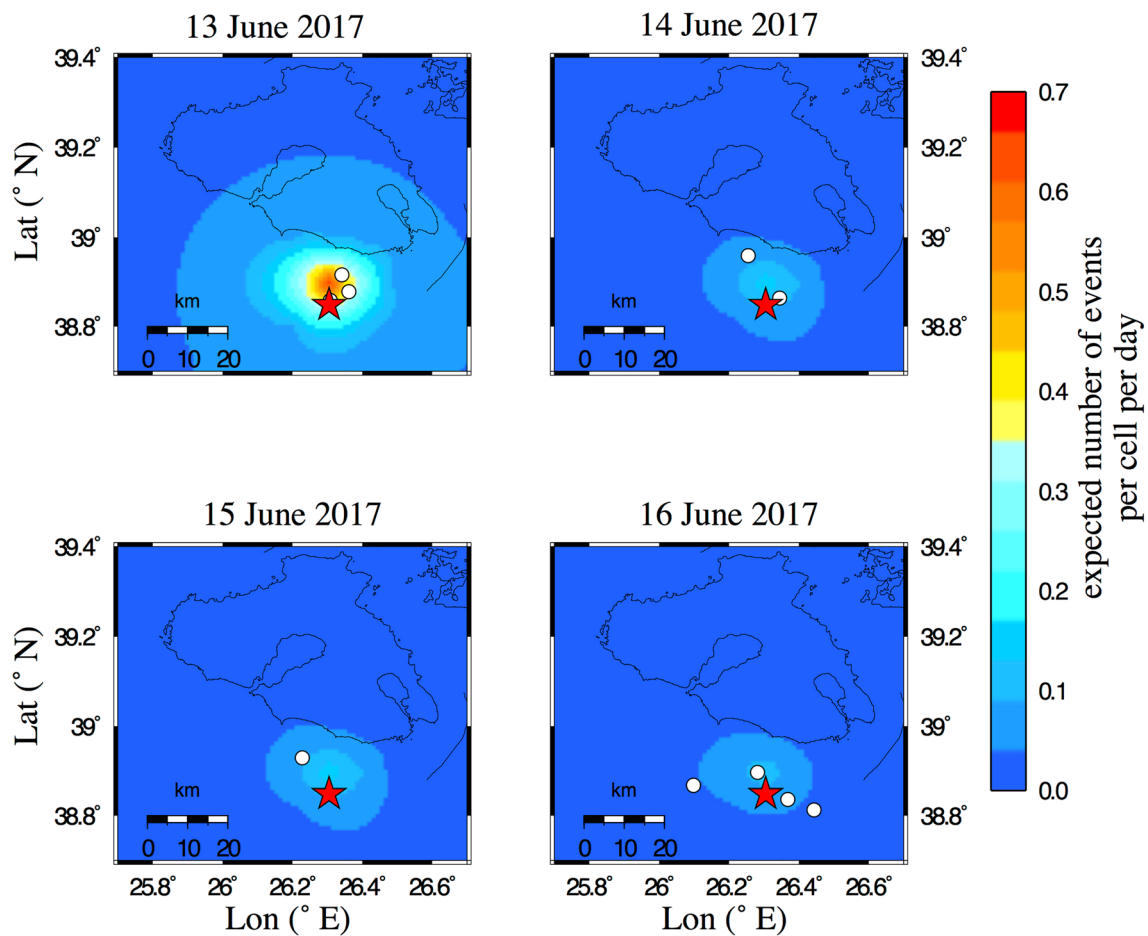


Fig. 12 Expected number of events with $M \geq 3.5$ related to the Lesvos sequence per day per cell of $0.1^\circ \times 0.1^\circ$ from 13 to 16 June 2017. The starting time for the daily computations is at midnight. The epicenters

of the occurring shocks are represented with white circles. The red star represents the epicenter of the $M_w = 6.4$ Lesvos earthquake that occurred on 12 June 2017

Table 5 Expected and observed number of events with $M \geq 3.5$ and $M \geq 4.5$ per day under the clustering model for Lesvos sequence

Date	Number of events with $M \geq 3.5$		Number of events with $M \geq 4.5$	
	Expected	Observed	Expected	Observed
12 June 2017	0.06	17	0.0035	1
13 June 2017	12.02	3	0.70	0
14 June 2017	5.14	2	0.30	0
15 June 2017	3.39	1	0.19	0
16 June 2017	2.56	6	0.15	0
17 June 2017	2.48	7	0.15	2

forecast of the model $M \geq 3.5$. Among the three sequences, the one located near Lesvos Island, presents the largest discrepancy in terms of the number of events. This may be due to the relatively high value of the magnitude threshold considered, according to which only events with $M \geq 3.1$

are capable to produce subsequent aftershocks while events with lower magnitude are not considered at all.

The results and the frequent occurrence of strong ($M_w \geq 6.0$) earthquakes in the study area highlight the need for the application of the model in real time. Daily forecasts would potentially allow us to investigate the variations of seismicity that will lead to the detection of increased potential foreshock activity a few hours before the occurrence of a strong event. The evolution of the aftershock activity could also be successfully tracked and become a powerful tool for decision makers.

Acknowledgements The constructive comments of two anonymous reviewers are greatly appreciated and contributed to the significant improvement of the manuscript. Gratitude is also extended to Prof. R. Zuniga for his editorial assistance. The earthquake catalogs of Geophysics Department of the Aristotle University of Thessaloniki are accessible from <http://geophysics.geo.auth.gr/ss> (last accessed December 2020). The GMT software (Wessel et al. 2013) is used for creating the maps. Some figures are created with the used of MATLAB software

(<http://www.mathworks.com/products/matlab>). Fault plane solutions data used in Figure 3 came from <https://www.globalcmt.org/> (last accessed December 2020). Geophysics Department Contribution 951.

Declarations

Conflict of Interest On behalf of all authors, the corresponding author states that there is no conflict of interest.

References

- Aki K (1965) Maximum likelihood estimate of b in formula $\log(N)=\alpha-bM$ and its confidence limits. *Bull Earthq Res Inst Univ Tokyo* 43:237–239
- Aristotle University of Thessaloniki (1981) Aristotle University of Thessaloniki seismological network. International Federation of Digital Seismograph Networks. <https://doi.org/10.7914/SN/HT>
- Console R, Murru M (2001) A simple and testable model for earthquake clustering. *J Geophys Res* 106:8699–8711
- Console R, Murru M, Lombardi AM (2003) Refining earthquake clustering models. *J Geophys Res* 108:2468
- Console R, Rhoades DA, Murru M, Evison FF, Papadimitriou EE, Karakostas VG (2006) Comparative performance of time-invariant, long range and short-range forecasting models on the earthquake catalogue of Greece. *J Geophys Res* 111:B09304. <https://doi.org/10.1029/2005JB004113>
- Console R, Murru M, Catalli F, Falcone G (2007) Real time forecasts through an earthquake clustering model constrained by the rate-and-state constitutive law: comparison with a purely stochastic ETAS model. *Seismol Res Lett* 78:49–56
- Console R, Jackson DD, Kagan YY (2010) Using the ETAS model for catalog declustering and seismic background assessment. *Pure Appl Geophys* 167:819–830
- de Arcangelis L, Godano C, Grasso JR, Lippiello E (2016) Statistical physics approach to earthquake occurrence and forecasting. *Phys Rep* 628:1–91. <https://doi.org/10.1016/j.physrep.2016.03.002>
- Field EH, Milner KR, Hardebeck JL, Page MT, van den Elst N, Jordan TH, Michael AJ, Shaw BE, Werner MJ (2017) A spatiotemporal clustering model for the third uniform California earthquake rupture forecast (UCERF3-ETAS): to-ward an operational earthquake forecast. *Bull Seismol Soc Am* 107:1049–1081. <https://doi.org/10.1785/0120160173>
- Frankel A (1995) Mapping seismic hazard in the central and eastern United States. *Seismol Res Lett* 66:8–21
- Ganas A, Elias P, Kapetanidis V, Valkaniotis S, Briole P, Kassaras I, Argyrakos P, Barberopoulou A, Moshou A (2018) The July 20, 2017 M6.6 Kos earthquake: seismic and geodetic evidence for an active north-dipping normal fault at the western end of the Gulf of Gokova (SE Aegean Sea). *Pure Appl Geophys* 176(10):4177–4211. <https://doi.org/10.1007/s00024-019-02154-y>
- Gospodinov D, Karakostas V, Papadimitriou E (2015) Seismicity rate modeling for prospective stochastic forecasting: the case of 2014 Kefalonia, Greece, seismic excitation. *Nat Hazards* 79:1039–1058. <https://doi.org/10.1007/s11069-015-1890-8>
- Gutenberg B, Richter C (1949) *Seismicity of the earth and associated phenomena*, 2nd edn. University Press, Princeton
- Helmstetter A, Jackson DD, Kagan YY (2006) Comparison of short-term and time-independent earthquake forecast models for southern California. *Bull Seismol Soc Am* 96:90–106
- Jordan T (2006) Earthquake predictability, brick by brick. *Seismol Res Lett* 77:3–6. <https://doi.org/10.1785/gssrl.77.1.3>
- Karakostas VG, Tan O, Kostoglou A, Papadimitriou EE, Bonatis P (2020) Seismotectonic implications of the 2020 Samos, Greece, M7.0 mainshock based on high-resolution aftershocks relocation, source slip model, and previous microearthquake activity. *Acta Geophys* (submitted)
- Kourouklas C, Mangira O, Iliopoulos A, Chorozoglou D, Papadimitriou E (2020) A study of short-term spatiotemporal clustering features of Greek seismicity. *J Seismol* 24:459–477. <https://doi.org/10.1007/s10950-020-09928-1>
- LePichon X, Angelier J (1979) The Hellenic Arc and Trench system: a key to the neotectonic evolution of the eastern Mediterranean area. *Tectonophysics* 60(1–2):1–42
- Lombardi AM, Cocco M, Marzocchi W (2010) On the increase of background seismicity rate during the 1997–1998 Umbria-Marche, central Italy, sequence: apparent variation or fluid-driven triggering? *Bull Seismol Soc Am* 100:1138–1152
- Mangira O, Console R, Papadimitriou E, Murru M, Karakostas V (2020) The short-term seismicity of the Central Ionian Islands (Greece) studied by means of a clustering model. *Geophys J Int* 220:856–875. <https://doi.org/10.1093/gji/gg481>
- Marzocchi W, Lombardi AM (2008) A double branching model for earthquake occurrence. *J Geophys Res* 113:317
- Marzocchi W, Lombardi AM (2009) Real-time forecasting following a damaging earthquake. *Geophys Res Lett* 36:L21302
- McClusky S, Balassanian S, Barka A, Demir C, Ergintav S, Georgiev I, Gurkan O, Hamburger M, Hurst K, Kahle H, Kastens K, Kekelidze G, King R, Kotzev V, Lenk O, Mahmoud S, Mishin A, Nadariya M, Ouzounis A, Paradisis D, Peter Y, Prilepin M, Reilinger R, Sanli I, Seeger H, Tealeb A, Toksöz MN, Veis G (2000) Global positioning system constraints on plate kinematics and dynamics in the eastern Mediterranean and Caucasus. *J Geophys Res* 105:5695–5719. <https://doi.org/10.1029/1999JB900351>
- Mesimeri M, Kourouklas C, Papadimitriou E, Karakostas V, Kementzetzidou D (2018) Analysis of microseismicity associated with the 2017 seismic swarm near the Aegean coast of NW Turkey. *Acta Geophys* 66:479–495. <https://doi.org/10.1007/s11600-018-0157-7>
- Murru M, Console R, Falcone G (2009) Real time earthquake forecasting in Italy. *Tectonophysics* 470:214–223
- Murru M, Zhuang J, Console R (2014) Falcone G (2014) Short-term earthquake forecasting experiment before and during the L'Aquila (central Italy) seismic sequence of April 2009. *Ann Geophys* 57:S0649. <https://doi.org/10.4401/ag-6583>
- Ogata Y (1983) Estimation of the parameters in the modified Omori formula for aftershock sequences by the maximum likelihood procedure. *J Phys Earth* 31:115–124
- Ogata Y (1988) Statistical models for earthquake occurrences and residual analysis for point processes. *J Am Stat Assoc* 83:9–27
- Ogata Y (1998) Space-time point-process models for earthquake occurrences. *Ann Inst Stat Math* 50:379–402
- Ogata Y (2011) Significant improvements of the space-time ETAS for forecasting of accurate baseline seismicity. *Earth Planets Space* 63:217–229. <https://doi.org/10.5047/eps.2010.09.001>
- Ogata Y, Zhuang J (2006) Space-time ETAS models and an improved extension. *Tectonophysics* 413:13–23. <https://doi.org/10.1016/j.tecto.2005.10.016>
- Ogata Y, Katsura K, Falcone G, Nanjo KZ, Zhuang J (2013) Comprehensive and topical evaluations of earthquake forecasts in terms of number, time, space, and magnitude. *Bull Seismol Soc Am* 103:1692–1708
- Omori F (1894) On the aftershocks of earthquakes. *J Coll Sci Imp Univ Tokyo* 7:111–200
- Papadimitriou P, Kassaras I, Kaviris G, Tselentis G-A, Voulgaris N, Lekkas E, Chouliaras G, Evangelidis C, Pavlou K, Kapetanidis V, Karakonstantis A, Kazantzidou-Firtinidou D, Fountoulakis I, Millas C, Spingos I, Aspiotis T, Moumoulidou A, Skourtsos E, Antoniou V, Andreadakis E, Mavroulis S, Kleanthi M (2018) The

- 12th June 2017 $M_w = 6.3$ Lesvos earthquake from detailed seismological observations. *J Geodyn* 115:23–42. <https://doi.org/10.1016/j.jog.2018.01.009>
- Papazachos BC, Comninakis PE (1971) Geophysical and tectonic features of the Aegean arc. *J Geophys Res* 76:8517–8533
- Papazachos BC, Karakaisis GF, Papadimitriou EE, Papaioannou CA (1997a) The regional time and magnitude predictable model and its application to the Alpine-Himalayan belt. *Tectonophysics* 271:295–323
- Papazachos BC, Kiratzi AA, Karakostas BG (1997b) Towards a homogeneous moment-magnitude determination for earthquakes in Greece and the surrounding area. *Bull Seismol Soc Am* 87:474–483
- Rhoades DA, Evison FF (2004) Long-range earthquake forecasting with every earthquake a precursor according to scale. *Pure Appl Geophys* 161:47–72
- Rhoades DA, Schorlemmer D, Gerstenberger MC, Christophersen A, Zechar JD, Imoto M (2011) Efficient testing of earthquake forecasting models. *Acta Geophys* 59:728–747
- Savran WH, Werner MJ, Marzocchi W, Rhoades DA, Jackson DD, Milner K, Field E, Michael A (2020) Pseudoprospective evaluation of UCERF3-ETAS forecasts during the 2019 Ridgecrest sequence. *Bull Seismol Soc Am* 110:1799–1817. <https://doi.org/10.1785/0120200026>
- Schorlemmer D, Werner MJ, Marzocchi W, Jordan TH, Ogata Y, Jackson DD, Mak S, Rhoades DA, Gerstenberger MC, Hirata N, Liukis M, Maechling PJ, Strader A, Taroni M, Wiemer S, Zechar JD, Zhuang J (2018) The collaboratory for the study of earthquake predictability: achievements and priorities. *Seismol Res Lett* 89(4):1305–1313. <https://doi.org/10.1785/0220180053>
- Shi Y, Bolt A (1982) The standard error of the magnitude-frequency b value. *Bull Seismol Soc Am* 72:1677–1687
- Tan O, Papadimitriou EE, Pabuccu Z, Karakostas V, Yoruk A, Lepitokarpoulos K (2014) A detailed analysis of microseismicity in Samos and Kusadasi (Eastern Aegean Sea) areas. *Acta Geophys* 62:1283–1309. <https://doi.org/10.2478/s11600-013-0194-1>
- Wessel P, Smith WHF, Scharroo R, Luis J, Wobbe F (2013) Generic mapping tools: improved version released. *EOS Trans Am Geophys Union* 94:409–410
- Wiemer S, Wyss M (2000) Minimum magnitude of completeness in earthquake catalogs: examples from Alaska, the western United States, and Japan. *Bull Seismol Soc Am* 90:859–869. <https://doi.org/10.1785/0119990114>
- Zechar JD, Schorlemmer D, Liukis M, Yu J, Euchner F, Maechling PJ, Jordan TH (2010) The collaboratory for the study of earthquake predictability perspective on computational earthquake science. *Concurr Comput Pract Exp* 22(12):1836–1847. <https://doi.org/10.1002/cpe.1519>
- Zhuang J, Ogata Y, Vere-Jones D (2002) Stochastic declustering of space-time earthquake occurrence. *J Am Stat Assoc* 97:369–380
- Zhuang J, Ogata Y, Vere-Jones D (2004) Analyzing earthquake clustering features by using stochastic reconstruction. *J Geophys Res* 109:B05301. <https://doi.org/10.1029/2003JB002879>
- Zhuang J, Chang C-P, Ogata Y, Chen Y-I (2005) A study of the background and clustering seismicity in the Taiwan region by using a point process model. *J Geophys Res* 110:B05S18. <https://doi.org/10.1029/2004JB003157>
- Zhuang J, Christophersen A, Savage MK, Vere-Jones DD (2008) Differences between spontaneous and triggered earthquakes. Their influences on foreshock probabilities. *J Geophys Res* 113:B11302
- Zhuang J, Murru M, Falcone G, Guo Y (2018) An extensive study of clustering features of seismicity in Italy from 2005 to 2016. *Geophys J Int* 216:302–318. <https://doi.org/10.1093/gji/ggy428>